Available online at www.sciencedirect.com
ScienceDirect
Earth and Planetary Science Letters 260 (2007) 72–85
EPSL
www.elsevier.com/locate/epsl

High-temperature Mars-to-Earth transfer of meteorite ALH84001

Kyoungwon Min [a,*], Peter W. Reiners [b]

[a] Department of Geological Sciences, University of Florida, 241 Williamson Hall, P.O. Box 112120, Gainesville, Florida 32611, United States
[b] Department of Geosciences, University of Arizona, Tucson, Arizona 85721, United States

Received 23 November 2006; received in revised form 10 May 2007; accepted 11 May 2007
Available online 23 May 2007
Editor: R.W. Carlson

Abstract

Martian meteorites provide crucial insights into Martian evolution and interplanetary mass transfer, including the potential for exogenesis. ALH84001 is the oldest Martian meteorite discovered so far, and has been used to derive important conclusions about Martian surface temperatures and very low-temperature Mars-to-Earth transfer. To better constrain the thermal evolution and shock metamorphic history of ALH84001, we applied (U–Th)/He thermochronometry to single grains of phosphate (merrillite) from ALH84001. The (U–Th)/He ages of individual phosphate grains in ALH84001 range from 60 Ma to 1.8 Ga, with a weighted mean of ~830 Ma. This broad age distribution reflects multiple diffusion domains, and requires a relatively high-temperature resetting event younger than ~ 60 Ma. These new data are combined with the published whole-rock (maskelynite as a main Ar reservoir) $^{40}Ar/^{39}Ar$ age spectra which show 5–8% fractional loss of radiogenic ^{40}Ar since 4.0 Ga. He diffusion in both terrestrial and extraterrestrial apatite has a significantly higher activation energy (138 ~ 184 kJ/mol) than Ar diffusion in maskelynite (75 kJ/mol), leading to an important "kinetic crossover" in fractional loss contours for these systems. Taken together, the phosphate (U–Th)/He and whole-rock $^{40}Ar/^{39}Ar$ ages require both very low surface temperatures on Mars, and one or more short-lived, high-temperature, shock events after 4.0 Ga. We suggest that the last shock event occurred with ejection of ALH84001 from Mars, and reached a peak temperature of approximately 400 °C. These results undermine the proposed low-temperature ejection hypothesis for ALH84001, but support long-lived extremely cold Martian surface temperatures.

Keywords: ALH84001; thermochronology; Martian meteorite; (U–Th)/He; phosphate

1. Introduction

Mars is thought to have experienced intense volcanism, impact cratering and fluvial resurfacing during its first ~1.5 Ga, followed by a less-energetic, colder period (Hartmann and Neukum, 2001). Rare meteoritic samples of the Martian crust (38 have been identified so far (Mars Meteorite Compendium)) provide some of the only direct evidence by which to test and develop models of the paleoenvironmental evolution of the planet, its potential habitability by life, and the process of interplanetary mass transport. Thermal histories of Martian meteorites provide crucial evidence bearing not only on long-term, ambient near-surface conditions on Mars (Shuster and Weiss, 2005), but also on whether meteoroids can be ejected from their large parent bodies without significant heating (Head et al., 2002), a favorable condition for exogenesis (including panspermia) hypotheses. One of the best samples to address these

* Corresponding author. Tel.: +1 352 392 2720.
E-mail address: kmin@ufl.edu (K. Min).

0012-821X/$ - see front matter © 2007 Elsevier B.V. All rights reserved.
doi:10.1016/j.epsl.2007.05.019

issues is Martian meteorite ALH84001, because it has the oldest crystallization age (~4.5 Ga: (Jagoutz et al., 1994; Nyquist et al., 1995)), is thought to have resided near the surface since ~4.0 Ga, and has been suggested to have experienced no significant heating during or after its ejection from Mars at 15 Ma (Kirschvink et al., 1997; Weiss et al., 2000).

ALH84001 is an igneous cumulate comprising mainly orthopyroxene and minor chromite, maskelynite, phosphate (chlorapatite and merrillite), augite, olivine, sulfide, carbonate and silica glass. After its formation at ~4.5 Ga, ALH84001 experienced an intense shock event at ~4.0 Ga, producing multiple fine-grained granular bands, transformation of feldspar crystals to maskelynite (Mittlefehldt, 1994; Treiman, 1995), and complete resetting of its $^{40}Ar/^{39}Ar$ system (Ash et al., 1996; Turner et al., 1997; Bogard and Garrison, 1999). The 4.0 Ga-shock was followed by formation of chemically-zoned carbonates in fractures, particularly in association with maskelynite (McKay et al., 1996; Scott et al., 1997; Kring et al., 1998). The Rb/Sr age of the carbonates is indistinguishable from the ~4.0-Ga $^{40}Ar/^{39}Ar$ age, suggesting the carbonate formation occurred immediately after the intense shock event (Borg et al., 1999).

The thermal history of ALH84001 after 4.0 Ga is controversial. Kirschvink et al. (1997) obtained stable, but slightly oblique NRM (Natural Remanent Magnetization) orientations from two adjacent pyroxene grains closely related to the carbonate-bearing globules, and suggested that this originates from post-shock cooling at 4.0 Ga. Because these magnetic properties disappear during minor heating in the laboratory, they argued that the carbonates formed at relatively low temperatures, and have not been heated above ~110 °C since formation at ~4.0 Ga. Weiss et al. (2000) found localized heterogeneous NRM orientations from two slabs of ALH84001, and concluded that internal parts of the meteorite have been below ~40 °C since before its ejection from Mars at ~15 Ma.

In contrast, petrographic evidence suggests at least one intense thermal event after carbonate formation. Treiman (1998) assigned two or three impact events to explain the observed melting of feldspar and the carbonates crosscut by microfaults (his D3), rotation of the magnetized grains (D4), and ejection from Mars (D5). As he noted, the D4 and D5 could be from a single impact event at ~15 Ma. Greenwood and McSween (2001) noticed some "old" feldspathic glass, presumably formed at 4.0 Ga, was intruded by another set of plagioclase-composition glass and silica veins with minor mobilization of the "old" feldspathic glasses and carbonates. According to these studies, all the petrographic and geochemical features can be explained by two shock events of pre- and post-carbonate formation. They also imply high pressure-temperature conditions (>~55 GPa) for the second shock, and the timing of the shock was conjectured to be ~15 Ma, the timing of ejection of ALH84001. These conclusions are not easily reconciled with the low-T ejection hypothesis suggested by Kirschvink et al. (1997).

The shock pressure and temperature conditions of ALH84001 were more quantitatively estimated based on the refractive index of maskelynite (diaplectic glass with feldspathic composition) and, at a lesser degree, using other textures such as planar fractures, mosaicism and undulose extinction. It is known that the refractive index of maskelynite in shocked meteorites systematically decreases as the shock pressure increases, and this relationship was calibrated using experimentally and naturally shocked materials (Stöffler, 1967; Gibbons and Ahrens, 1977; Ostertag, 1983; Stöffler et al., 1986; Bischoff and Stöffler, 1992). Once pressure is determined from the refractive index of maskelynite, corresponding shock temperature is deduced from the equation of state (EOS) of terrestrial materials with compositions similar to the extraterrestrial target phases (Stöffler, 1982; Artemieva and Ivanov, 2004). Based on this calibration and petrographic observations, it was suggested that ALH84001 experienced shock metamorphism corresponding to 35–40 GPa and ~300–400 °C post-shock temperature (temperature increase during a shock event) (Stöffler, 2000; Nyquist et al., 2001). However, recent advances of the calibration yielded significantly reduced shock conditions of 32±1 GPa and 105±5 °C (Fritz et al., 2005). The large discrepancy, particularly in temperature estimates, is yet to be resolved.

Another approach to constraining the thermal history is through $^{40}Ar/^{39}Ar$ thermochronometry. Turner et al. (1997) obtained $^{40}Ar/^{39}Ar$ data from three subparts of ALH84001, and determined Ar diffusion parameters and age spectra. Using these diffusion parameters and volume diffusion theory, they modeled the age spectra, concluding that ALH84001 had not been heated significantly since 4.0 Ga. Weiss et al. (2002) took a similar approach, using previously published $^{40}Ar/^{39}Ar$ data (Bogard and Garrison, 1999), and suggested that ALH84001 was never heated above 350–500 °C since carbonate formation at 4.0 Ga. Shuster and Weiss (2005), however, showed that the $^{40}Ar/^{39}Ar$ data can be explained by a wide range of long-term thermal histories, in which temperature and time are traded off against one another. According to their calculations, although a history of ~4.0 Ga of holding at ~−60 °C was consistent with the data, a transient thermal event with a maximum

temperature as high as 500 °C could not be ruled out, if its duration was short (e.g., less than a few hours). Therefore, the $^{40}Ar/^{39}Ar$ data for ALH84001 can broadly constrain durations, timing and temperatures of thermal histories and pulses, but does not discriminate between the two opposing hypotheses of high-*T* and low-*T* ejection at 15 Ma, which is critical to understanding impact dynamics, interplanetary material transfer, and exogenetic potential.

To better constrain the thermal evolution and shock metamorphic history of ALH84001, we applied (U–Th)/He thermochronometry to single grains of phosphate from ALH84001.

2. Analytical methods

Approximately 1.2 g of a rock chip (ALH84001, 34, originally from ALH84001, 14) was gently crushed and sieved, and grains were spread on double-sided carbon tape and analyzed using ESEM (Environmental Scanning Electron Microscopy) for chemical and morphological examinations. The grains were scanned for 2-dimensional chemical mapping of several elements, and phosphate grains were identified using the compositional distribution of P and Ca. For those identified as phosphates, qualitative spot analyses were undertaken with EDS (Energy Dispersion Spectroscopy). All the observed phosphate grains contain detectable Mg and Fe, and no Cl, suggesting chemical composition of merrillite. All the observed phosphate grains have other phases attached, and these phases (e.g., orthopyroxene) are readily distinguished from phosphates by their chemical compositions (Fig. 1). In many cases, the size of an individual phosphate was close to the size of its host grain, although there are a few exceptions, for which phosphates comprised as little as 20% of the grain. Phosphate-bearing grains greater than ~80 μm were retrieved for further measurements of ^{4}He, U, Th and Sm concentrations.

The samples were wrapped with Pt tubes and heated using a Nd-YAG laser for 3 min. Liberated gas was spiked with ^{3}He, and He was concentrated and purified, and ^{4}He contents were measured by quadrupole mass spectrometry. Reheating and reextractions were performed on three samples, yielding negligible amounts (<0.5% of the previous degassing) of ^{4}He. The degassed sample packages were retrieved, spiked with ^{229}Th and ^{233}U, and the phosphate portions were dissolved from their foil packets by nitric acid. U, Th, and Sm were quantified by isotope dilution on a sector ICP–MS. Details of analytical procedures are available in (Min et al., 2004).

Whereas He diffusion in terrestrial apatite is well documented (Farley, 2000; Shuster et al., 2006), the thermal sensitivity of He diffusion in meteoritic phosphates is not well known. No He diffusion data, for example, are available for merrillite, the most abundant phosphate in ALH84001. Although it is impossible to precisely estimate diffusion parameters without performing diffusion experiments, it is likely that the diffusion properties of merrillite are similar to those of terrestrial apatite, for the following reasons.

First, the kinetics of fission track annealing and He diffusion scale fairly systematically among diverse phases, both terrestrial and extraterrestrial, supporting comparable He diffusion characteristics for apatite and merrillite. For example, ^{244}Pu fission track retention temperatures (temperatures at which 50% of the original fission tracks are retained) for both merrillite and apatite in meteorites are suggested to be 117±15 °C at rapid cooling rates (8–20 °C/Ma), based on empirical calibration (Pellas and Storzer, 1981). Mold et al. (1984) performed a series of annealing experiments on chlorapatite and merrillite from Estacado chondrite (H6) and concluded that merrillite has slightly higher annealing temperature (84±10 °C) than chlorapatite (66±10 °C) at a cooling rate of 1 °C/Ma. These estimates were revised by Pellas et al. (1997) to 115±25 °C and 81±20 °C for merrillite and apatite, respectively. The updated annealing temperature of merrillite was used by Trieloff et al. (2003) to infer cooling histories of various H chondrites. For terrestrial samples, the U fission track annealing temperatures show a general trend of zircon (~230–310 °C (Tagami and Dumitru, 1996; Hasebe et al., 2003)) ≥ titanite (200–280 °C (Harrison et al., 1979)) > apatite (60–120 °C (Green et al., 1989; Corrigan, 1993)). The same trend is observed for He closure temperatures: zircon (~180 °C (Reiners et al., 2004)) ≥ titanite (~180 °C (Reiners and Farley, 1999)) > apatite (~70 °C (Farley, 2000)) (all closure temperatures cited for grains with a diffusion domain radius of 200 μm and a cooling rate of 1 °C/Ma). Although there is no clear theoretical grounds for such systematic variation between the track annealing kinetics and He diffusion, it is likely that track annealing is essentially limited by diffusion of interstitial atoms and similar crystallographic phenomena as He diffusion. If the observed relationship for fission track annealing and He diffusion can be extended to merrillite, the He closure temperature of merrillite is expected to be similar to, or slightly higher than that of apatite. We note that He ages of merrillite in the Los Angeles Martian meteorite were slightly older than those of apatite (Min et al., 2004).

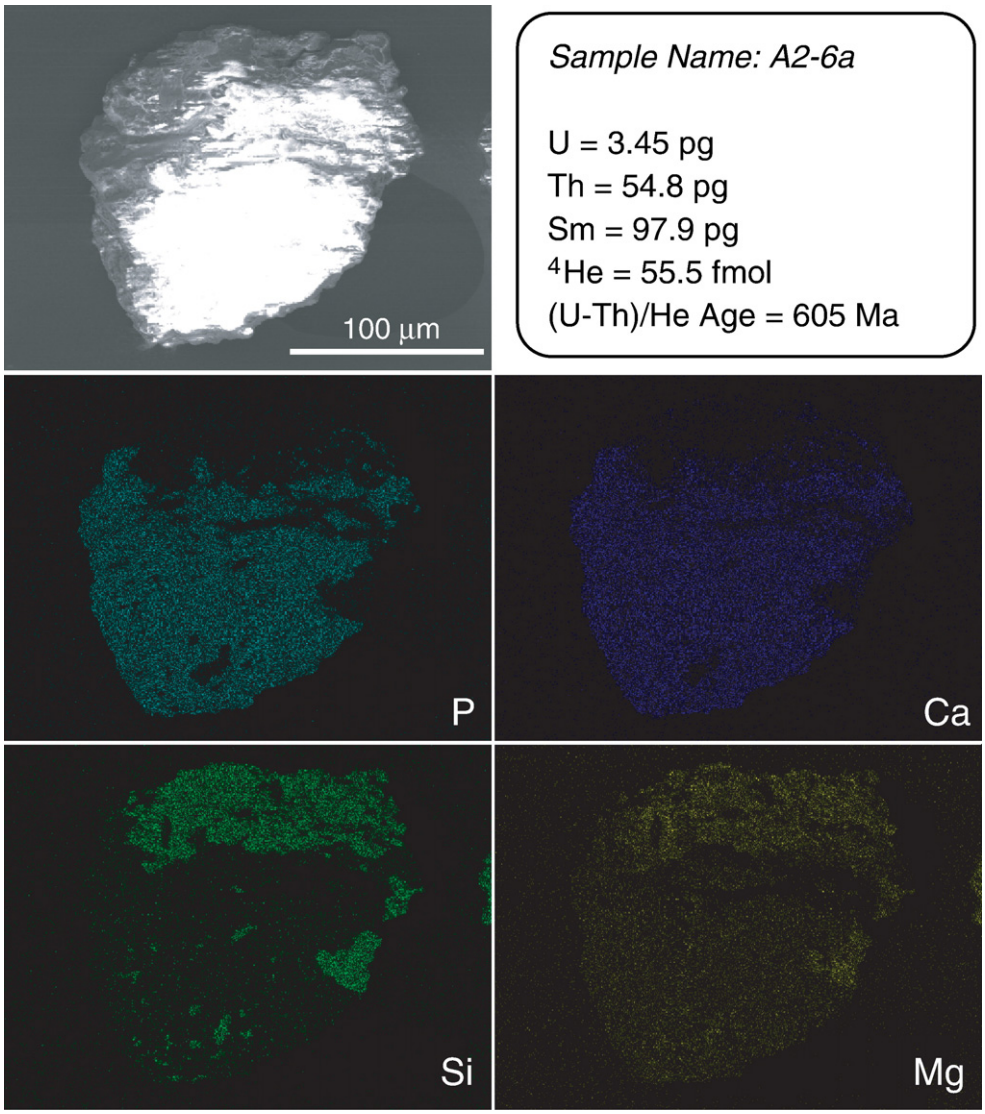

Fig. 1. Distribution of four different elements (P, Ca, Si and Mg) on surface of a phosphate grain, A2-6a. The main body (center and bottom) of the grain has high P- and Ca-contents consistent with a phosphatic composition. The top part of the grain is orthopyroxene with Si and Mg. All other phosphate grains contain silicate minerals (mainly orthopyroxene) on their surfaces.

Second, both merrillite $[(Ca,REE)_{18}(Mg, Fe, Mn)_2 Na_{2-x}(PO_4)_{14}]$ and apatite $[Ca_5(PO_4)_3(OH, F, Cl)]$ have very similar ionic porosities (Z). Because the ionic porosity is a good proxy for the mean atomic packing density of a mineral, it has long been suspected that the ionic porosity may be one of the main factors controlling volume diffusion (Dowty, 1980). As high quality experimental results became available, strong linear correlations between ionic porosity (Z) and diffusion parameters (E and $\log(D_o)$) were successfully documented for various diffusants in a wide variety of host phases (Fortier and Giletti, 1989; Dahl, 1996a, b; Dahl, 1997; Zheng and Fu, 1998; Zhao and Zheng, 2007). The ionic porosity of merrillite is ~45.2 based on the recent crystallographic studies on extraterrestrial samples (Jolliff et al., 2006; Hughes et al., 2006) combined with crystal radii (Shannon, 1976; Http://abulafia.mt.ic.ac.uk/shannon/). This estimate is essentially identical with the values estimated for apatite (44.8–45.4 (Zhao and Zheng, 2007)), and such results strongly support similar He diffusion kinetics for the two minerals. Because of these reasons and lack of He diffusion data

on merrillite, we assumed that the merrillite has the same diffusion properties as those of the Durango apatite (Farley, 2000) for the thermal modeling in this paper.

Alpha recoil correction is generally required for most terrestrial samples based on grain morphologies (Farley et al., 1996) because they are chosen partly for their good crystal shapes, thus their original dimensions and geometries are likely to have been preserved during sample preparation. For meteoritic samples such as these, however, alpha recoil is both more difficult to apply, and likely to be less important, because most of the dated phosphate grains are either from internal parts of the originally large crystals or from grains with other phases, which capture He ejected from the attached phosphate sources (Min et al., 2003; Min et al., 2004; Min, 2005). Nonetheless, if we assume complete preservation of original crystal shapes and no other phases on grain surfaces, application of alpha recoil corrections to these grains, while increasing ages by ~95% on average, has a minimal effect on the main interpretations of this work, only lowering the maximum post shock temperature by ~50 °C. However, as noted above, this estimate is based on a highly unlikely scenario, thus should be considered as a hypothetical end-member value. We consider the uncorrected ages much more robust, and use them throughout this paper.

The cosmogenic component of ^{4}He was estimated using the production rate of 80.5 ncc/g-Ma (Eugster, 1988) and an exposure age of 15 Ma (Nyquist et al., 2001), and this contribution is generally extremely small (Table 1). A complete data set is available in Table 1.

3. Results

Thirty two phosphate grains yielded (U–Th)/He ages widely scattered in the range of 57 Ma–1.8 Ga (standard deviation = 460 Ma) with one outlier at 3.4 Ga (Fig. 2,

Table 1
(U–Th)/He data for phosphates in ALH84001 Martian meteorite

Sample name	U (pg)	Th (pg)	Sm (pg)	Th/U atomic ratio	^{4}He total (fmol)	^{4}He$_{cosmo}$	(U–Th)/He age (Ma)	1σ (Ma)	1σ (%)
2A1-3a	1.01	7.32	27.2	7.42	21.4	0.07%	1330	51	3.8%
2A1-3b	0.48	3.63	10.1	7.70	3.81	0.12%	508	34	6.8%
2A1-6a	0.58	10.4	8.85	18.5	66.1	0.00%	3420	140	4.1%
2A1-7a	32.3	90.0	305	2.85	379	0.02%	1190	22	1.8%
2A1-7b	0.42	11.1	26.2	27.1	11.5	0.15%	669	23	3.5%
2A1-9a	1.42	19.3	54.2	14.0	52.4	0.03%	1500	42	2.8%
2A1-10a	1.28	23.2	30.8	18.5	28.2	0.05%	745	18	2.4%
A1-4a	3.91	61.5	152	16.1	53.9	0.10%	524	9.8	1.9%
A2-6a	3.45	54.8	97.9	16.3	55.5	0.08%	605	11	1.9%
2A2-3a	6.18	47.2	161	7.85	122	0.03%	1210	37	3.0%
2A2-8a	4.83	17.0	65.9	3.62	68.1	0.03%	1290	68	5.2%
2A2-12a	0.98	2.94	14.2	3.08	6.72	0.13%	699	170	24%
2A2-13a	2.19	5.62	23.8	2.63	7.27	0.07%	370	43	12%
2B1-6a	4.37	27.3	72.1	6.42	65.4	0.03%	1050	45	4.3%
2B1-7a	0.80	6.63	23.8	8.55	13.4	0.04%	989	170	17%
2B1-7b	1.22	5.52	20.0	4.63	13.0	0.03%	897	150	17%
2B1-7c	2.05	6.40	31.8	3.21	27.8	0.02%	1300	160	12%
2B1-8a	2.12	6.85	105	3.32	1.19	0.63%	56.6	5.9	11%
2B1-8d	0.53	2.28	1.23	4.43	3.80	0.20%	632	240	38%
2B1-9a	1.82	35.2	67.1	19.9	51.2	0.01%	894	40	4.5%
2B1-13b	1.19	7.33	30.1	6.29	27.0	0.01%	1540	230	15%
2B1-10a	2.67	26.3	81.9	10.1	27.1	0.19%	543	27	4.9%
2B2-13a	12.2	60.8	49.6	5.11	54.9	0.04%	373	8.9	2.4%
2B3-10a	5.18	36.8	84.5	7.29	77.2	0.01%	970	34	3.5%
2B3-10b	2.52	24.2	31.3	9.85	30.6	0.01%	661	35	5.3%
A3A1-12a	0.63	8.10	31.9	13.2	16.1	0.03%	1110	100	9.0%
A3A1-12b	15.1	84.0	69.2	5.70	31.7	0.02%	166	3.0	1.8%
A3A2-11a	1.91	22.0	49.0	11.9	13.0	0.11%	331	11	3.2%
A3A2-11b	12.3	8.10	10.8	0.68	8.65	0.02%	112	3.1	2.7%
A3b1-3a	3.84	26.0	72.8	6.94	15.9	0.01%	288	7.4	2.6%
A3b1-6a	0.21	5.16	14.6	25.7	15.0	0.02%	1810	260	14%
A3b1-11a	1.67	5.54	13.3	3.39	5.49	0.03%	333	22	6.7%

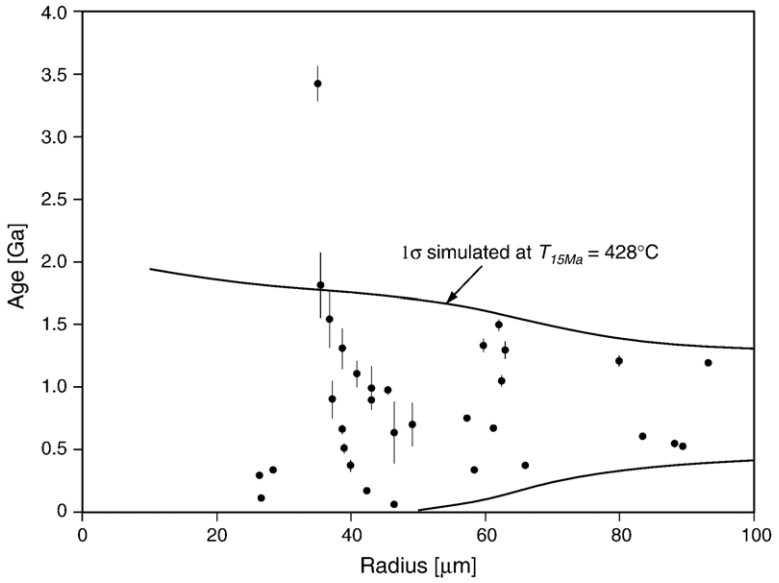

Fig. 2. Single-grain phosphate (U–Th)/He ages (Table 1) and sizes of grains from ALH84001 Martian meteorite. There is no positive relationship between sample size and He age, and the degree of age scatter decreases as the sample size increases. These observations are consistent with each sample representing multiple diffusion domains or parts of them, as illustrated in Fig. 3. The curves represent 1-sigma uncertainty simulated with the observed diffusion domain size distribution (Fig. 5) and assuming a single shock event at 15 Ma ($T_{15\ Ma}$=428 °C) since 4.0 Ga (see text for details). The simulation generally resembles the actual data suggesting that the wide age distribution is due to multi-domain diffusion. The ages are shown with 1-sigma analytical uncertainties.

Table 1). The weighted mean age (without the single outlier) is 830 Ma, corresponding to a He fractional loss of 84% since 4.0 Ga. The single-grain phosphate ages show a similar range as previously reported whole rock (U–Th)/He ages of 0.3–1.2 Ga of ALH84001 (Swindle et al., 1995).

4. Interpretation and discussion

4.1. Age distribution modeling

The most likely explanation for the wide range of He ages is that the phosphate (U–Th)/He system was partially reset by one or more events, and that this range reflects variations in the sampling of different parts, sizes, and aggregates of diffusion domains in each grain. Fig. 2 shows that there is no simple (positive or negative) relationship between age and size of each phosphate. This means that individual grains cannot be regarded as single, entire diffusion domains because such conditions would result in a positive age–size relationship by partial resetting. Instead, the individual grains are more likely parts of larger diffusion domains or aggregates of multiple diffusion domains with different domain sizes (Fig. 3). This is also supported by the observation that the degree of age scatter decreases as the sample size increases (Fig. 2). An alternative, but less likely hypothesis to explain the widely scattered age distribution is that the shock waves have caused very heterogeneous impact on the target material resulting in different degrees of He loss over even a few micrometer scale. However, there is no proven example of such heterogeneous effect on He loss or transient changes in He diffusion properties during the passage of shock waves. In this paper, we assumed that the He diffusion was mainly controlled by homogeneous temperature rise on the entire parent meteoroid of ALH84001 followed by conductive cooling.

Both step-heating diffusion experiments and microscopic observations have been used to model Ar diffusion domain distributions in terrestrial alkali feldspars (Lovera et al., 1991; Fitz Gerald and Harrison, 1993). In contrast to the complicated internal structures of alkali feldspar, phosphate (mainly apatite) crystals have simpler microtextures allowing more straightforward diffusion modeling for He diffusion. Both diffusion experiments and dating results show that terrestrial phosphate crystals are generally single diffusion domains (Farley, 2000; Reiners and Farley, 2001). Even for extraterrestrial phosphates, He diffusion appears to follow simple Arrhenius relationships suggesting thermally-activated volume diffusion (Min et al., 2003). These lines of evidence imply that He

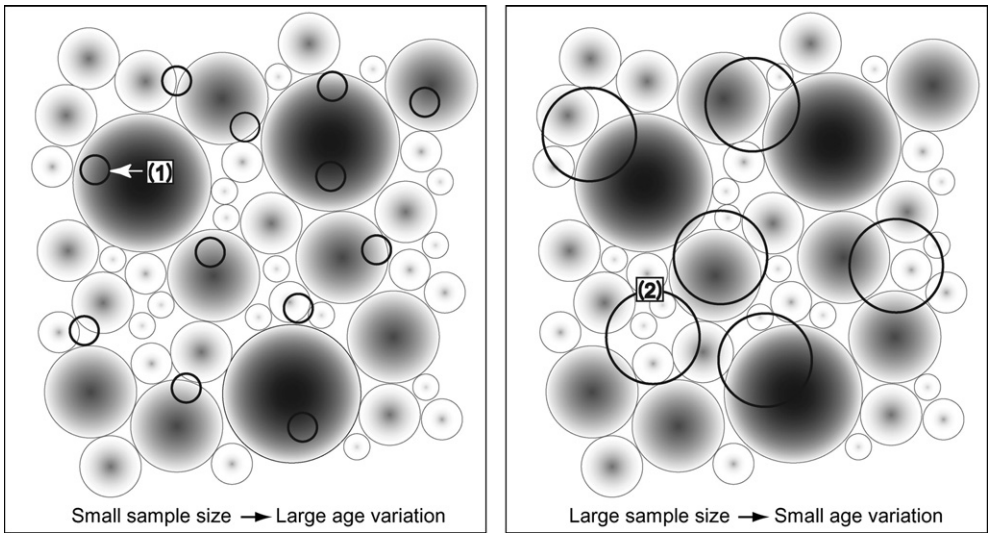

Fig. 3. Cartoons illustrating the schematic relationship between analyzed samples (circles with thick boundaries) and diffusion domains (circles with thin boundaries). The gradient shade inside of the diffusion domains represents schematic He distribution (darker shade represents higher He concentration) after partial degassing. The sample circles may consist of a part of a large diffusion domain (e.g., (1) in the figure) or multiple domains (e.g., (2)). Smaller samples collect limited portions of the whole, producing more heterogeneous (U–Th)/He ages.

diffusion in phosphate crystals is less complicated than Ar diffusion in terrestrial alkali feldspars, and can be used for age modeling if the internal domain structure of the grains is understood.

Interpreting the phosphate He ages requires understanding the nature of their diffusion domains. We carefully examined back-scattered electron (BSE) images of five ALH84001 phosphate grains described in Greenwood et al. (2003). All these grains have numerous, relatively thick fractures (maximum width > ~1–2 μm), which likely represent routes of fast He diffusion, and therefore bound effective He diffusion domains (Fig. 4a). If these fractures existed prior to, or formed contemporaneously with, the last major thermal event to affect the He ages, then the effective diffusion domains for the He ages recorded in these grains are smaller than the individual crystals, and their sizes can be estimated from the fracture-free areas (FFA) in the BSE images. One hundred thirty two FFAs were defined for these grains (Fig. 4b), and each FFA was converted into a radius of a circle with a corresponding surface area measured in the BSE images.

The estimated radii of FFAs vary widely from ~1 to 40 μm with one exceptionally large one of ~54 μm (Fig. 5). The most representative radius (peak of the weighted radius distribution) of the effective diffusion domains is in the range of 25–30 μm. In order to test our hypothesis that the observed age distribution is due to sampling a range of parts and aggregates of partially reset diffusion domains of varying sizes, we calculated He fractional loss (f_{He}) for the observed fracture-free area (FFA) distribution. As discussed in the following section, for this modeling we assumed a partial resetting event at 15 Ma, with a peak temperature of 428 °C. Because each of our individual phosphate-bearing grains represents a (U–Th)/He age of a part of a larger diffusion domain or an aggregate of multiple domains, it is necessary to model each analysis as a random collection of diffusion domains of variable sizes following the observed distribution.

To estimate the most likely age distribution from the observed size distribution of FFA, the following calculation steps were performed. (1) Once He loss in individual diffusion domains was determined, we modeled their effects on He age distributions by randomly locating them in 2-dimensional space (as in the illustrations in Fig. 3). (2) For a given sample size, an arbitrary position was chosen in the 2-dimensional space as a center of a sample circle. (3) A sample circle was gradually increased from the center until the overlap with the nearby diffusion domains became the given size (area) of the sample. Therefore, even for a given sample size, the radius of a sample circle can be variable depending on the locations of the sample circle and diffusion domains. (4) The He concentration (and fractional loss f_{He}) within the sample circle was calculated by simply summing the numbers of He atoms in all overlapped areas. (5) A standard deviation of the resulting f_{He} values was calculated. (6) Steps (2)–(5) were repeated 10,000 times until the calculated standard deviation of f_{He}

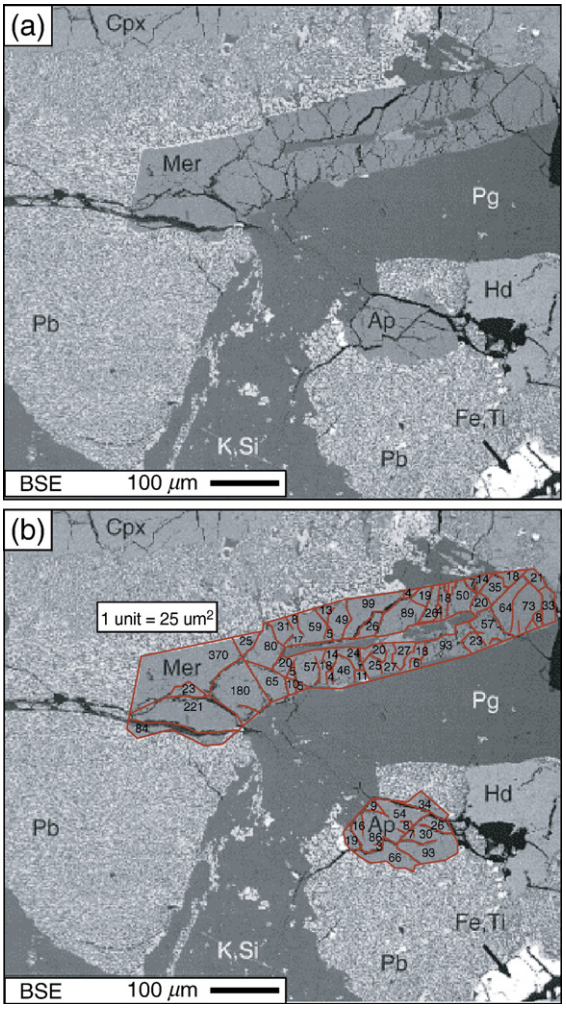

Fig. 4. (a) A Back-scattered electron (BSE) image containing a large merrillite and one smaller apatite crystals (Fig. 1 in Greenwood et al., 2003). These phosphate crystals have numerous fractures with maximum width of > ~ 1–2 μm. (b) For these crystals, fracture-free areas (FFAs) were defined and each FFA's 2-dimensional surface area was measured (as shown with numbers: 1 unit = 25 μm^2).

became stable within ~1%. (7) For different sample sizes, Steps (2)–(6) were repeated.

The curves in Fig. 2 show the resulting standard deviations estimated for different sample sizes (0–100 μm in radius), and these curves follow the general trend in the observed data. Larger grains are more likely to approximate the average diffusion domain size and therefore age, than smaller ones.

4.2. Thermal evolution of ALH84001

He diffusion in both terrestrial and extraterrestrial apatite has a significantly higher activation energy (138–184 kJ/mol: (Farley, 2000; Min et al., 2003)) than Ar diffusion in maskelynite (75 kJ/mol: (Weiss et al., 2002)), leading to an important "kinetic crossover" in fractional loss contours for these systems (Fig. 6). At low temperatures, He diffusion in phosphate is slower than Ar diffusion in maskelynite, but at higher temperatures this is reversed. The important result is that only short-duration reheating events at relatively high temperature can cause greater fractional loss of He in phosphate than Ar in maskelynite. For complete degassing (complete age resetting), or for equal extents of fractional resetting in both systems, this kinetic crossover occurs at approximately 150 °C. In the case of incomplete resetting of both systems by a single reheating event, the combined temperature and duration of the event can be estimated (Fig. 6). The curves are only strictly valid for a thermal event that ended at the present (or the very recent past), and they need to be corrected for He and Ar ingrowth following thermal events in the past. However, only a minor correction is required if the thermal event occurred recently (e.g., 15 Ma), relative to the primary reset age of 4.0 Ga.

As shown in Fig. 6, the observed 5–8% Ar loss in maskelynite in ALH84001 (Weiss et al., 2002) could be interpreted as low-temperature (e.g., ~−63 °C) degassing over extremely long durations (e.g., 4 Ga) or by higher temperature degassing for shorter durations (Shuster and Weiss, 2005). However, at low temperatures, essentially no He loss from phosphate will occur, even over extremely long time intervals (Fig. 6). For example, −63 °C for 4 Ga induces less than 0.1% He loss in phosphate, much lower than the observed value of 84%. To produce 84% He loss over a 4 Ga duration, the temperature would have to be ~17 °C, but this would lead to complete Ar loss in maskelynite. Therefore, a continuous degassing scenario during prolonged, low-temperature evolution fails to simultaneously explain the observed He and Ar data.

A more likely thermal history to explain both the He and Ar data from ALH84001 may be a single, recent heating event with an integrated Dt/a^2 equivalent to a square pulse event at slightly less than 400 °C for ~1 h (e.g., intersection of the ~84% He loss and 5–8% Ar loss in Fig. 6). The only reasonable geologic process corresponding to such a short and high temperature episode is a shock metamorphic event, which is commonly associated with ejection of meteoroids from their large parent bodies. The broad distribution of the (U–Th)/He ages suggests the thermal event was not intense enough to completely reset the He ages, and the timing of such event should be *younger* than ~60 Ma, the youngest single-grain (U–Th)/He age. We suggest

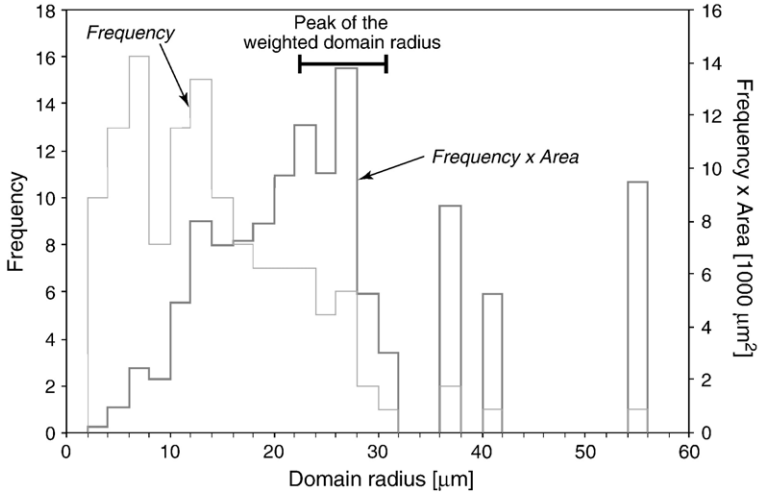

Fig. 5. Distribution of FFA (fracture-free area) radii. After 132 FFAs were defined in five merrillite and apatite grains described in Greenwood et al. (2003), their 2-dimensional surface areas were measured and converted to radii (blocks with thin boundaries). Most of the FFA radii are < 42 μm with one exceptionally large one (54 μm). Because a contribution of small domain (FFA) to the sample age is smaller than that of larger domain, the frequency was weighted by the 2-dimensional surface areas observed from individual FFAs. The bold blocks represent the area-weighted frequency (frequency × area). The most representative domain radius of ~ 25–30 μm was deduced form the area-weighted distribution.

that the simplest explanation involves a 15 Ma shock event associated with the ejection of ALH84001 from Mars.

The thermal history resulting from shock metamorphism almost certainly followed a conductive cooling history (Weiss et al., 2000; Min et al., 2004) rather than a

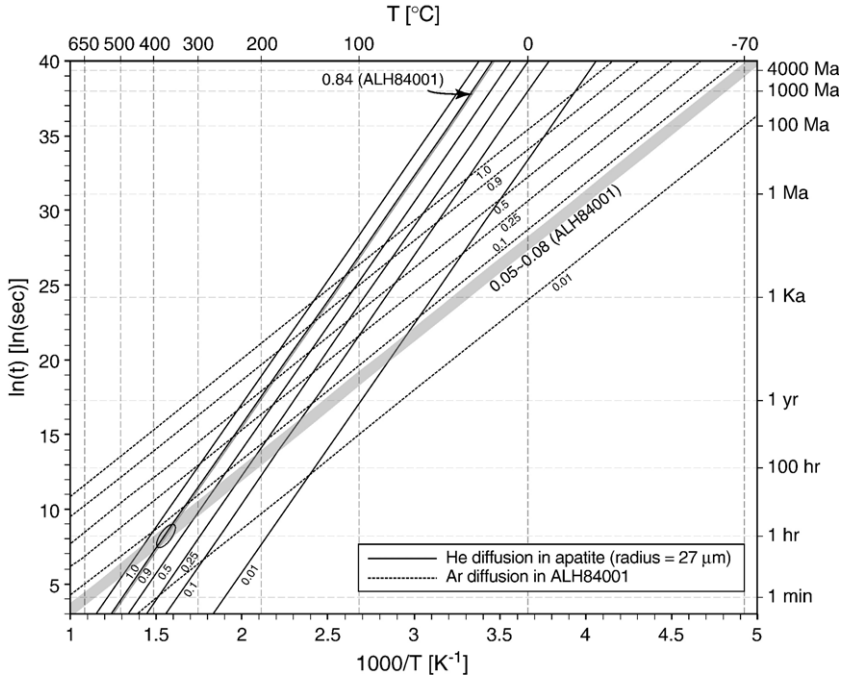

Fig. 6. Contours of fractional loss of He in phosphate (solid curves) and Ar in maskelynite (dotted curves), for thermal events of different temperature and time. He diffusion parameters are for Durango apatite Farley (2000) and Ar for bulk ALH84001 (Weiss et al., 2002). The slopes for He fractional loss contours are steeper than those for Ar, because of the relatively low activation energy of Ar diffusion in maskelynite. This means that the maskelynite Ar system is sensitive to the sample's long-term, low-temperature history, whereas the phosphate He system is sensitive to short-duration, high-temperature events. Only short-duration, high-temperature events can cause phosphate (U–Th)/He ages to be younger than maskelynite $^{40}Ar/^{39}Ar$ ages. The curves corresponding to the observed fractional losses for He (0.84) and Ar (0.05–0.08) intersect at $T \sim 350$–400 °C and $t \sim 1$ h, as marked with an ellipse.

square heat pulse. Initially we employed a conductive cooling model with an assumption that all the observed radiogenic ^{4}He and ^{40}Ar were lost by a single shock event at 15 Ma after their accumulation since 4.0 Ga. For the diffusion modeling, we used a pre-atmospheric body radius of 10 cm (Goswami et al., 1997), depth of the sample from the surface of pre-atmospheric body of 7 cm (5 cm (ablation depth deduced from cosmogenic noble gases and nuclear tracks: (Goswami et al., 1997)) +2 cm (distance from the surface of the present ALH84001)), the surface temperature of −70 °C, diffusion domain radius of 27 μm, thermal diffusivity of 0.01 cm^2/s and diffusion parameters of Farley (2000). The model calculation gives a peak temperature ($T_{15\ Ma}$) of ~428 °C to explain the observed f_{He} of 84% (this study), and this estimate yields f_{Ar} of 6.3%, well within the observed range of 5–8% (Weiss et al., 2002; Shuster and Weiss, 2005). The estimated peak temperature of 428 °C has a large uncertainty mainly due to uncertainties in input parameters. If a pre-atmospheric body radius of 20 cm is used (Weiss et al., 2002), instead of our favored estimate of 10 cm (Goswami et al., 1997), the model yields a $T_{15\ Ma}$ of ~360 °C which is ~70 °C lower than the previous estimate.

This model shock temperature for the 15 Ma event is probably a maximum estimate because other natural processes may have caused partial He and Ar losses during the short residence on Earth (~11 Ka), passage from Mars to Earth (~15 Ma), or long, low-temperature residence on Mars (~4.0 Ga) which is especially important for Ar diffusion. Its residence in Antarctica for 11 Ka at −10 °C would induce negligible fractional losses for He (<0.1%) and Ar (<0.2%). Another possible source of partial resetting is solar heating during the meteorite's journey from Mars to the Earth. According to the simulation of Gladman (1997), most Martian meteoroids stayed near the orbit of Mars during the early stage (~0.1 Ma) of wandering, and slowly diffused farther out, increasing orbital eccentricities to Earth-crossing values within several million years. If ALH84001 spent most of this time between the orbits of Mars and Earth, its temperature was usually below 0 °C, the temperature of a chondrite-colored body at 1 AU from the Sun (Butler, 1966). For various temperatures (−40 ~ 0 °C) and durations (1 Ka–10 Ma), we calculated isothermal fractional losses of He and Ar (Table 2). Although we modeled the f_{Ar} and f_{He} for wide temperature–duration conditions, many of these hypothetical conditions yield f_{Ar} exceeding the observed values of 5–8%, thus these conditions are not likely. The calculated f_{He} values for acceptable temperature–duration conditions do not exceed ~0.1%, ruling out

Table 2
f_{Ar} in maskelynite and f_{He} in merrillite expected for isothermal heating at given temperature–duration conditions

Total heating duration	Heating temperature											
	−50°C		−40°C		−30°C		−20°C		−10°C		0°C	
	f_{Ar}	f_{He}	f_{Ar}	f_{He}	f_{Ar}	f_{He}	f_{Ar}	f_{He}	f_{Ar}	f_{He}	f_{Ar}	f_{He}
0.001 Ma	<0.1%	<0.1%	<0.1%	<0.1%	0.1%	<0.1%	0.3%	<0.1%	<0.1%	<0.1%	1.1%	<0.1%
0.01 Ma	<0.1%	<0.1%	0.2%	<0.1%	0.4%	<0.1%	0.9%	<0.1%	1.7%	<0.1%	3.3%	<0.1%
0.1 Ma	0.2%	<0.1%	0.6%	<0.1%	1.3%	<0.1%	2.8%	<0.1%	5.5%	<0.1%	10.2%	0.1%
1 Ma	0.8%	<0.1%	1.8%	<0.1%	4.1%	<0.1%	8.6%	<0.1%	16.7%	0.1%	30.4%	0.3%
10 Ma	2.4%	<0.1%	5.7%	<0.1%	12.6%	<0.1%	25.7%	0.1%	47.4%	0.3%	76.3%	1.1%

Forbidden conditions with f_{Ar} >8% are marked with shade.

solar heating in space as a cause of significant He diffusion in phosphate.

It is possible, however, that ALH84001 experienced another thermal event on Mars sometime between 4.0 Ga and 15 Ma. To constrain the properties of such a hypothetical event, we modeled relationships among four different parameters: the 15-Ma shock temperature ($T_{15\ Ma}$), the timing of the pre-15 Ma isothermal event (t_1), and the temperature (T_1) and duration (dt_1) of the pre-15 Ma event. The curves in Fig. 7 represent the minimum $T_{15\ Ma}$ required to yield the observed (U–Th)/He ages if the thermal event ending at t_1 completely reset all the phosphate He systems. The area above the dashed curve represents possible combinations of $T_{15\ Ma}$ and t_1 if the pre-15 Ma event caused only partial He resetting, to yield the oldest age of 1810 Ma (except the anomalously old He age of 3420 Ma) or younger. The area above the solid curve in Fig. 7 corresponds to ages equal to or younger than 830 Ma, the weighted mean He age. For example, as shown with the solid curve in Fig. 7, if there was a complete resetting of He at 1 Ga (t_1), the 15 Ma shock temperature ($T_{15\ Ma}$) has to have been ~340 °C to yield the mean He age of 830 Ma, at the representative diffusion domain radius (27 μm). Therefore, the area above the dashed curve can explain most of the observed He ages (≤1810 Ma), whereas the area below is not acceptable. The "acceptable" area is defined by these two end members (dashed curve and horizontal line at 428 °C), and the "forbidden" conditions by the area below the dashed curve (marked with

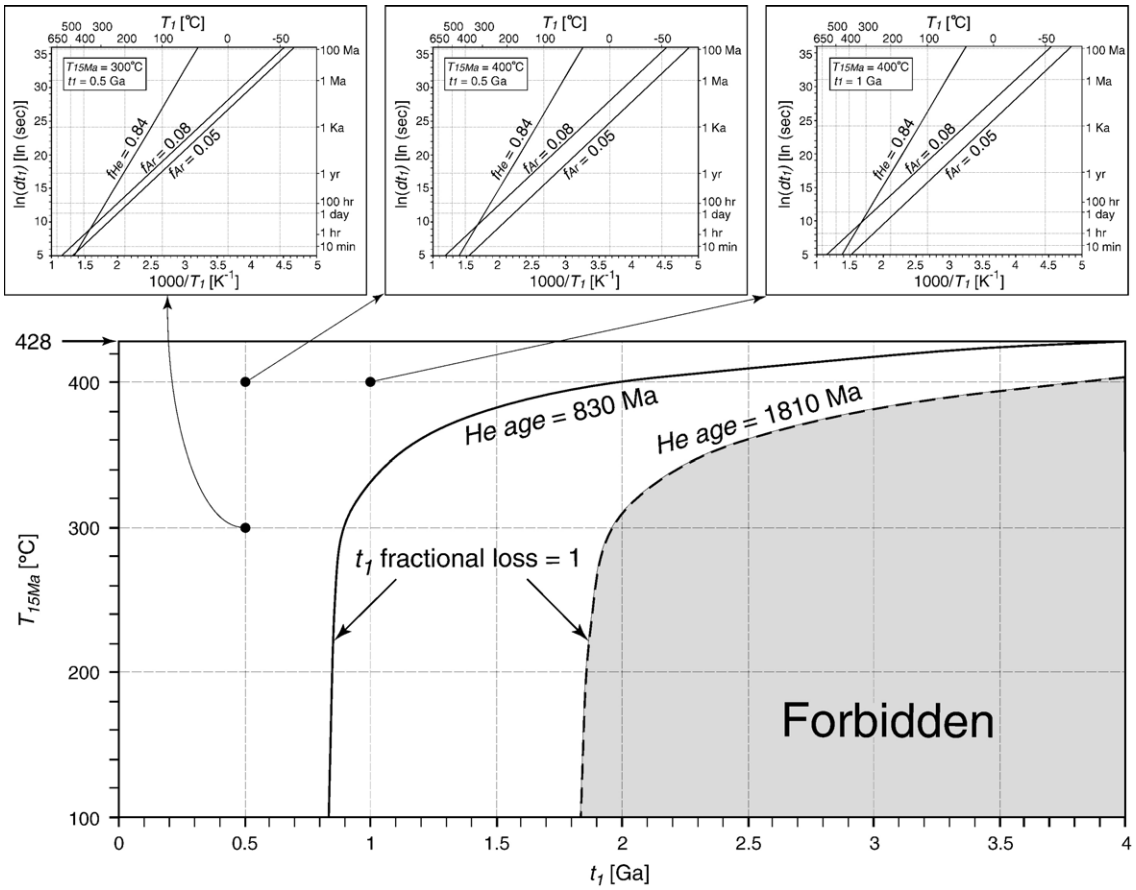

Fig. 7. Relationship between $T_{15\ Ma}$ (temperature of the 15 Ma event) and t_1 (the timing of a hypothetical pre-15 Ma thermal event). The dashed curve represents a minimum $T_{15\ Ma}$ at a certain t_1 where the complete He degassing occurred, to yield the oldest age of 1810 Ma. The area above this curve represents partial degassing at t_1, thus yielding the observed He ages (≤ 1810 Ma). Multiple curves can be drawn for different He ages. The solid curve is one example with 830 Ma, the weighted mean He age. The area above the solid curve corresponds to ages equal to or younger than 830 Ma. The maximum $T_{15\ Ma}$ of 428 °C was calculated based on the weighted mean He age (830 Ma) and most representative diffusion domain radius (27 μm), with a single He loss event at 15 Ma (without any other thermal disturbance since 4.0 Ga). The area below the dashed curve represents He ages > 1810 Ma, thus it is "forbidden". The anomalously old He age of 3420 Ma was excluded in constraining the relationship between $T_{15\ Ma}$ and t_1. Three insets show inverse relationship between T_1 and dt_1 for arbitrarily chosen points in the acceptable area. For these and other acceptable conditions, the solutions can be found in high-temperature, short-duration regions.

shade). The acceptable area becomes narrower as t_1 increases, indicating tighter constraints on $T_{15\ Ma}$ with older thermal episodes, and vice versa. It is noteworthy that the available He data have significantly large "forbidden" area in the $T_{15\ Ma}-t_1$ space, whereas Ar degassing curve is close to the vertical line at $t_1=4.0$ Ga, thus does not yield useful constraints on the $T_{15\ Ma}-t_1$ relationship.

For three arbitrary points in the acceptable $T_{15\ Ma}-t_1$ area in Fig. 7, we calculated temperature (T_1) and duration (dt_1) of a hypothetical pre-15 Ma event using the available He and Ar data. The resulting inverse relationship between T_1 and dt_1 for each point is shown in the insets. As explained in the Fig. 6, solutions can be found where the two He and Ar curves intersect. For variable points in the "acceptable" $T_{15\ Ma}-t_1$ area, the intersects in T_1-dt_1 space are located at high-T_1 and low-dt_1 regions suggesting the pre-15 Ma, post-4.0 Ga thermal event, if it occurred, must have lasted only for a few hours or less at several hundred degrees. This event may correspond to the D2 or D3 of Treiman (1998), who suggested multiple shock events on ALH84001.

5. Summary

Because of the strong kinetic contrast in He and Ar diffusion properties in phosphate and maskelynite, respectively, combined He and Ar data from ALH84001 provide constraints on both long-term ambient conditions, and require at least one short duration, high temperature event after ~4.0 Ga. The simplest explanation for the latter is a single shock metamorphic event at 15 Ma (the cosmogenic exposure age) with peak temperature of approximately 400 °C followed by conductive cooling within a short (<1 h) period.

Except during the high-temperature event(s), for most of its post −4.0 Ga history, ALH84001 must have been very cold, as Shuster and Weiss (2005) noted based on the Ar systematics. In order to accommodate the 15-Ma heating event (and possible earlier ones), the long-term (~4 Ga) holding temperature estimate needs to be slightly lower than their estimate of −63 °C (close to −70 °C). Because the source area of ALH84001 on Mars is unclear, it is hard to directly infer the average Martian surface temperature from the available data, but these results are generally consistent with an average surface temperature of Mars for the past 4 Ga that is comparable to the present-day average value (approximately −60 °C for the equatorial region and lower for higher latitudes).

Our findings are consistent with previous results (Shuster and Weiss, 2005) requiring very cold conditions (~−70 °C) for most of ALH84001's post −4.0 Ga history, but our conclusions are not consistent with those based on paleomagnetic observations, that the meteorite was not heated above ~110 °C for any duration since 4.0 Ga.

Acknowledgements

We thank Richard Ketcham for modifying a previous version the HeFTy program, and Stefan Nicolescu for analytical assistance. Constructive reviews by Mario Trieloff and an anonymous reviewer greatly improved the original manuscript. NASA kindly provided the ALH84001 sample. This work was funded by NSF grant EAR-0236965 to PWR.

References

Artemieva, N., Ivanov, B.A., 2004. Launch of Martian meteorites in oblique impacts. Icarus 171, 84–101.

Ash, R.D., Knott, S.F., Turner, G., 1996. A 4-Gyr shock age for a Martian meteorite and implications for the cratering history of Mars. Nature 380, 57–59.

Bischoff, A., Stöffler, D., 1992. Shock metamorphism as a fundamental process in the evolution of planetary bodies: information from meteorites. Eur. J. Mineral. 4, 707–755.

Bogard, D.D., Garrison, D.H., 1999. Argon-39–argon-40 "ages" and trapped argon in Martian shergottites, Chassigny, and Allan Hills 84001. Meteorit. Planet. Sci. 34, 451–473.

Borg, L.E., Connelly, J.N., Nyquist, L.E., Wiesmann, Shih H., Reese, Y., 1999. The age of the carbonates in Martian meteorite ALH84001. Science 286, 90–94.

Butler, C.P., 1966. Temperatures of meteoroids in space. Meteoritics 3, 59–70.

Corrigan, J.D., 1993. Apatite fission track analysis of Oligocene strata in South Texas, USA: testing annealing models. Chem. Geol. 104, 227–249.

Dahl, P.S., 1996a. The effects of composition on retentivity of argon and oxygen in hornblende and related amphiboles: a field-tested empirical model. Geochim. Cosmochim. Acta 60, 3687–3700.

Dahl, P.S., 1996b. The crystal-chemical basis for Ar retention in micas: inferences from interlayer partitioning and implications for geochronology. Contrib. Mineral. Petrol. 123, 22–39.

Dahl, P.S., 1997. A crystal-chemical basis for Pb retention and fission track annealing systematics in U-bearing minerals, with implications for geochronology. Earth Planet. Sci. Lett. 150, 277–290.

Dowty, E., 1980. Crystal–chemical factors affecting the mobility of ion in minerals. Am. Mineral. 65, 174–182.

Eugster, O., 1988. Cosmic-ray production rates for ^{3}He, ^{21}Ne, ^{38}Ar, ^{83}Kr, and ^{126}Xe in chondrites based on ^{81}Kr–Kr exposure ages. Geochim. Cosmochim. Acta 52, 1649–1662.

Farley, K.A., 2000. Helium diffusion from apatite: General behavior as illustrated by Durango fluorapatite. J. Geophys. Res. 105, 2903–2914.

Farley, K.A., Wolf, R.A., Silver, L.T., 1996. The effects of long alpha-stopping distances on (U–Th)/He ages. Geochim. Cosmochim. Acta 60, 4223–4229.

Fortier, S.M., Giletti, B.J., 1989. An empirical model for predicting diffusion coefficients in silicate minerals. Science 245, 1481–1484.

Fritz, J., Artemieva, N., Greshake, A., 2005. Ejection of Martian meteorites. Meteorit. Planet. Sci. 40, 1393–1411.

Fitz Gerald, J.D., Harrison, T.M., 1993. Argon diffusion domains in K-feldspar I: microstructures in MH-10. Contrib. Mineral. Petrol. 113, 367–380.

Gibbons, R.V., Ahrens, T.J., 1977. Effects of shock pressures on calcic plagioclase. Phys. Chem. Miner. 1, 95–107.

Gladman, B., 1997. Destination: Earth Martian meteorite delivery. Icarus 130, 228–246.

Goswami, J.N., Sinha, N., Murty, S.V.S., Mohapatra, R.K., Clement, C.J., 1997. Nuclear tracks and light noble gases in Allan Hills 84001: preatmospheric size, fall characteristics, cosmic-ray exposure duration and formation age. Meteorit. Planet. Sci. 32, 91–96.

Green, P.F., Duddy, I.R., Laslett, G.M., Hegarty, K.A., Gleadow, A.J.W., Lovering, J.F., 1989. Thermal annealing of fission tracks in apatite 4. Quantitative modeling techniques and extension to geologic time-scales. Chem. Geol. 79, 155–182.

Greenwood, J.P., McSween Jr., H.Y., 2001. Petrogenesis of Allan Hills 84001: constraints from impact-melted feldspathic and silica glasses. Meteorit. Planet. Sci. 36, 43–61.

Greenwood, J.P., Blake, R.E., Coath, C.D., 2003. Ion microprobe measurements of $^{18}O/^{16}O$ ratios of phosphate minerals in the Martian meteorites ALH84001 and Los Angeles. Geochim. Cosmochim. Acta 67, 2289–2298.

Harrison, T.M., Armstrong, R.L., Naeser, C.W., Harakal, J.E., 1979. Geochronology and thermal history of the Coast pluton complex, near Prince Rupert, British Columbia. J. Earth Sci. 16, 400–410.

Hartmann, W.K., Neukum, G., 2001. Cratering chronology and the evolution of Mars. Space Sci. Rev. 96, 165–194.

Hasebe, N., Mori, S., Tagami, T., Matsui, R., 2003. Geological partial annealing zone of zircon fission-track system: additional constraints from the deep drilling MITI-Nishikubiki and MINI-Mishima. Chem. Geol. 199, 45–52.

Head, J.N., Melosh, H.J., Ivanov, B.A., 2002. Martian meteorite launch: High-speed ejecta from small craters. Science 298, 1752–1756.

http://abulafia.mt.ic.ac.uk/shannon/.

Hughes, J.M., Jolliff, B.L., Gunter, M.E., 2006. The atomic arrangement of merrillite from the Fra Mauro Formation, Apollo 14 Lunar mission: the first structure of merrillite from the Moon. Am. Mineral. 91, 1547–1552.

Jagoutz, E., Sorowka, A., Vogel, J.D., Wänke, H., 1994. ALH84001: Alien or progenitor of the SNC family? Meteoritics 29, 478 (Abstract).

Jolliff, B.L., Hughes, J.M., Freeman, J.J., Zeigler, R.A., 2006. Crystal chemistry of lunar merrillite and comparison to other meteoritic and planetary suites of whitlockite and merrillite. Am. Mineral. 91, 1583–1595.

Kirschvink, J.L., Maine, A.T., Vali, H., 1997. Paleomagnetic evidence of a low-temperature origin of carbonate in the Martian meteorite ALH84001. Science 275, 1629–1633.

Kring, D.A., Swindle, T.D., Gleason, J.D., Grier, J.A., 1998. Formation and relative ages of maskelynite and carbonate in ALH84001. Geochim. Cosmochim. Acta 62, 2155–2166.

Lovera, O.M., Richter, F.M., Harrison, T.M., 1991. Diffusion domains determined by ^{39}Ar released during step heating. J. Geophys. Res. 96, 2057–2069.

Mars Meteorite Compendium, http://www-curator.jsc.nasa.gov/curator/..%5Cantmet/mmc/index.cfm.

McKay, D.S., Gibson Jr., E.K., Thomas-Keprta, K.L., Vali, H., Romanek, C.S., Clemett, S.J., Chillier, X.D.F., Maechling, C.R., Zare, R.N., 1996. Search for past life on Mars: possible relic biogenic activity in Martian meteorite ALH84001. Science 273, 924–930.

Min, K., 2005. Low-temperature thermochronometry of meteorites. In: Reiners, P.W., Ehlers, T.A. (Eds.), Reviews in Mineralogy and Geochemistry: Low-Temperature Thermochronology, pp. 567–588.

Min, K., Farley, K.A., Renne, P.R., Marti, K., 2003. Single grain (U–Th)/He ages from phosphates in Acapulco meteorite and implications for thermal history. Earth Planet. Sci. Lett. 209, 323–336.

Min, K., Reiners, P.W., Nicolescu, S., Greenwood, J.P., 2004. Age and temperature of shock metamorphism of Martian meteorite Los Angeles from (U–Th)/He thermochronometry. Geology 32, 677–680.

Mittlefehldt, D.W., 1994. ALH84001, a cumulate orthopyroxenite member of the martian meteorite clan. Meteoritics 29, 214–221.

Mold, P., Bull, R.K., Durrani, S.A., 1984. Fission-track annealing characteristic of meteoritic phosphates. Nucl. Tracks 9, 119–128.

Nyquist, L.E., Bansal, B.M., Wiesmann, H., Shih, C.-Y., 1995. "Martians" young and old: Zagami and ALH84001 (abstract), Lunar Planet. Sci. XXVI, 1065–1066.

Nyquist, L.E., Bogard, D.D., Shih, C.-Y., Greshake, A., Stöffler, D., Eugster, O., 2001. Ages and geologic histories of Martian meteorites. Space Sci. Rev. 96, 105–164.

Ostertag, R., 1983. Shock experiments on feldspar crystals. J. Geophys. Res. 88, B364–B376.

Pellas, P., Storzer, D., 1981. ^{244}Pu fission track thermometry and its application to stony meteorites. Proc. R. Soc. London A 374, 253–270.

Pellas, P., Fiéni, C., Trieloff, M., Jessberger, E.K., 1997. The cooling history of the Acapulco meteorite as recorded by the ^{244}Pu and ^{40}Ar–^{39}Ar chronometers. Geochim. Cosmochim. Acta 61, 3477–3501.

Reiners, P.W., Farley, K.A., 1999. Helium diffusion and (U–Th)/He thermometry of titanite. Geochim. Cosmochim. Acta 63, 3845–3859.

Reiners, P.W., Farley, K.A., 2001. Influence of crystal size on apatite (U–Th)/He thermochronology: an example from the Bighorn Mountains, Wyoming. Earth Planet. Sci. Lett. 188, 413–420.

Reiners, P.W., Spell, T.L., Nicolescu, S., Zanetti, K.A., 2004. Zircon (U–Th)/He thermochronometry: He diffusion and comparison with $^{40}Ar/^{39}Ar$ dating. Geochim. Cosmochim. Acta 68, 1857–1887.

Shannon, R.D., 1976. Revised effective ionic radii and systematic studies of interatomic distances in halides and chalcogenides. Acta Crystallogr. A32, 751–767.

Scott, E.R.D., Yamaguchi, A., Krot, A.N., 1997. Petrological evidence for shock melting of carbonates in the Martian meteorite ALH84001. Nature 387, 377–379.

Shuster, D.L., Weiss, B.P., 2005. Martian surface paleotemperatures from thermochronology of meteorites. Science 309, 594–597.

Stöffler, D., 1967. Deformation und Umwandlung von Plagioklas durch Stoßwellen in den Gesteinen des Nördlinger Ries. Contrib. Mineral. Petrol. 16, 51–83.

Stöffler, D., 1982. Density of minerals and rocks under shock compression. In: Berlin, A.G. (Ed.), Landolt–Börnstein-Natural Data and Functional Relationships in Science and Technology. Springer, pp. 120–183.

Stöffler, D., 2000. Maskelynite confirmed as diaplectic glass: Indication for peak shock pressure below 45 GPa in all Martian meteorites. Lunar Planet. Sci. XXXI, 1170 (abstract).

Stöffler, D., Ostertag, R., Jammes, C., Pfannschmidt, G., Sen Gupta, P.R., Simon, S.M., Papike, J.J., Beauchamp, R.H., 1986. Shock metamorphism and petrography of the Shergotty achondrite. Geochim. Cosmochim. Acta 50, 889–903.

Shuster, D.L., Flowers, R.M., Farley, K.A., 2006. The influence of natural radiation damage on helium diffusion kinetics in apatite. Earth Planet. Sci. Lett. 249, 148–161.

Swindle, T.D., Grier, J.A., Burkland, M.K., 1995. Noble gases in orthopyroxenite ALH84001: a different kind of Martian meteorite with an atmospheric signature. Geochim. Cosmochim. Acta 59, 793–801.

Tagami, T., Dumitru, T.A., 1996. Provenance and thermal history of the Franciscan accretionary complex: constraints from zircon fission track thermochronology. J. Geophys. Res. 101, 11353–11364.

Treiman, A.H., 1995. A petrographic history of Martian meteorite ALH84001: two shocks and an ancient age. Meteoritics 30, 294–302.

Treiman, A.H., 1998. The history of Allan Hills 84001 revisited: multiple shock events. Meteorit. Planet. Sci. 33, 753–764.

Trieloff, M., Jessberger, E.K., Herrwerth, I., Hopp, J., Fiéni, C., Ghélis, M., Bourot-Denise, M., Pellas, P., 2003. Structure and thermal history of the H-chondrite parent asteroid revealed by thermochronometry. Nature 422, 502–506.

Turner, G., Knott, S.F., Ash, R.D., Gilmour, J.D., 1997. Ar–Ar chronology of the Martian meteorite ALH84001: evidence for the timing of the early bombardment of Mars. Geochim. Cosmochim. Acta 61, 3835–3850.

Weiss, B.P., Kirschvink, J.L., Baudenbacher, F.J., Vali, H., Peters, N.T., Macdonald, F.A., Wikswo, J.P., 2000. A low temperature transfer of ALH84001 from Mars to earth. Science 290, 791–795.

Weiss, B.P., Shuster, D.L., Stewart, S.T., 2002. Temperature on Mars from $^{40}Ar/^{39}Ar$ thermochronology of ALH84001. Earth Planet. Sci. Lett., vol. 201, pp. 465–472.

Zhao, Z.-F., Zheng, Y.-F., 2007. Diffusion compensation for argon, hydrogen, lead, and strontium in minerals. Am. Mineral. 92, 289–308.

Zheng, Y.-F., Fu, B., 1998. Estimation of oxygen diffusivity from anion porosity in minerals. Geochem. J. 32, 71–89.